Materials Letters 214 (2018) 60–63

Contents lists available at ScienceDirect

Materials Letters

journal homepage: www.elsevier.com/locate/mlblue

Electrospun $Ti_2Nb_{10}O_{29}$ hollow nanofibers as high-performance anode materials for lithium-ion batteries

Qingfeng Fu [a,b,c], Jingrong Hou [a,b,c], Ruohan Lu [a,b,c], Chunfu Lin [a,b,c,*], Yu Ma [a,b,c], Jianbao Li [b,c], Yongjun Chen [b,c]

[a] Key Laboratory of Advanced Materials of Tropical Island Resources (Hainan University), Ministry of Education, Haikou 570228, China
[b] State Key Laboratory of Marine Resource Utilization in South China Sea, Haikou 570228, China
[c] College of Materials and Chemical Engineering, Hainan University, Haikou 570228, China

ARTICLE INFO

Article history:
Received 19 August 2017
Received in revised form 15 November 2017
Accepted 18 November 2017
Available online 21 November 2017

Keywords:
Energy storage and conversion
Fibre technology
Nanocrystalline materials
Ceramics
$Ti_2Nb_{10}O_{29}$
Co-electrospinning

ABSTRACT

$Ti_2Nb_{10}O_{29}$ is a high-capacity, safe and stable anode material for lithium-ion batteries, but suffers from a poor rate capability. To tackle this issue, nanotechnology is employed, and $Ti_2Nb_{10}O_{29}$ hollow nanofibers with an average fiber diameter of ~500 nm and shell thickness of ~90 nm are prepared by a facile co-electrospining technique followed by calcination in air. This material exhibits not only a high reversible capacity (307 mAh g^{-1} at 0.1 C) and durable cyclic stability (0.06% capacity loss *per* cycle at 10 C over 500 cycles) but also an outstanding rate capability (136 mAh g^{-1} at 20 C), thereby becoming a promising anode material for high-performance lithium-ion batteries.

1. Introduction

The demand for safe lithium-ion batteries (LIBs) with high energy and power density for electric vehicles (EVs) is rapidly increasing [1]. Many efforts have been paid to the search for high-performance anode materials of LIBs in the past two decades [2–4]. Among the developed anode materials, intercalating $Ti_2Nb_{10}O_{29}$ holds a great perspective on a promising candidate to replace the commonly used graphite anode material due to its high theoretical/practical capacity (396/~300 mAh g^{-1}) based on its multiple redox couples (Ti^{3+}/Ti^{4+}, Nb^{3+}/Nb^{4+} and Nb^{4+}/Nb^{5+}) and a safe working potential (~1.7 V *vs.* Li/Li^+) inhibiting the electrolyte decomposition and lithium-dendrite formation [5]. Nevertheless, the main obstacle for the practical application of $Ti_2Nb_{10}O_{29}$ is its poor rate capability associated with its poor electronic/ionic conductivity. To overcome this obstacle, one of the most effective methods is to decrease the $Ti_2Nb_{10}O_{29}$ particle sizes to nanometer scale since the electrochemical-reaction areas of the $Ti_2Nb_{10}O_{29}$ nanomaterials are large and the electron/Li^+-ion transport distances within them are short. So far, however, very limited studies in this field have been reported [6,7].

Hollow nanostructures, with shell permeability and large surface areas, have attracted increasing research interest due to their fascinating properties, but have rarely been applied in LIBs [8]. In this work, we employ a facile co-electrospinning method to successfully synthesize pure $Ti_2Nb_{10}O_{29}$ hollow nanofibers for the first time. Besides the common merits of nanomaterials, the hollow nanofibers further provide extra space for the Li^+-ion storage, efficient electron transport along the nanofibers and significant pseudocapacitive behavior. Consequently, this material exhibits outstanding electrochemical performance in term of a high reversible capacity, safe working potential, high initial Coulombic efficiency, superior rate capability and advanced cyclic stability.

2. Results and discussion

The crystal structure and phase purity of the $Ti_2Nb_{10}O_{29}$ hollow nanofibers are examined by powder X-ray diffraction (XRD). As can be seen in Fig. 1a, all the XRD peaks are highly consistent with $Ti_2Nb_{10}O_{29}$ (JCPDS No. 72–159), suggesting that the Ti–Nb–O/PVP precursor is completely transformed into $Ti_2Nb_{10}O_{29}$ after the calcination. $Ti_2Nb_{10}O_{29}$ has a monoclinic shear ReO_3 crystal structure (the *A2/m* space group) constructed by $3 \times 4 \times \infty$ octahedron-blocks, in which the octahedra share the corners and/or edges (Fig. 1b), guaranteeing the good structural stability

* Corresponding author.
E-mail address: linchunfu@hainu.edu.cn (C. Lin).

https://doi.org/10.1016/j.matlet.2017.11.076
0167-577X/

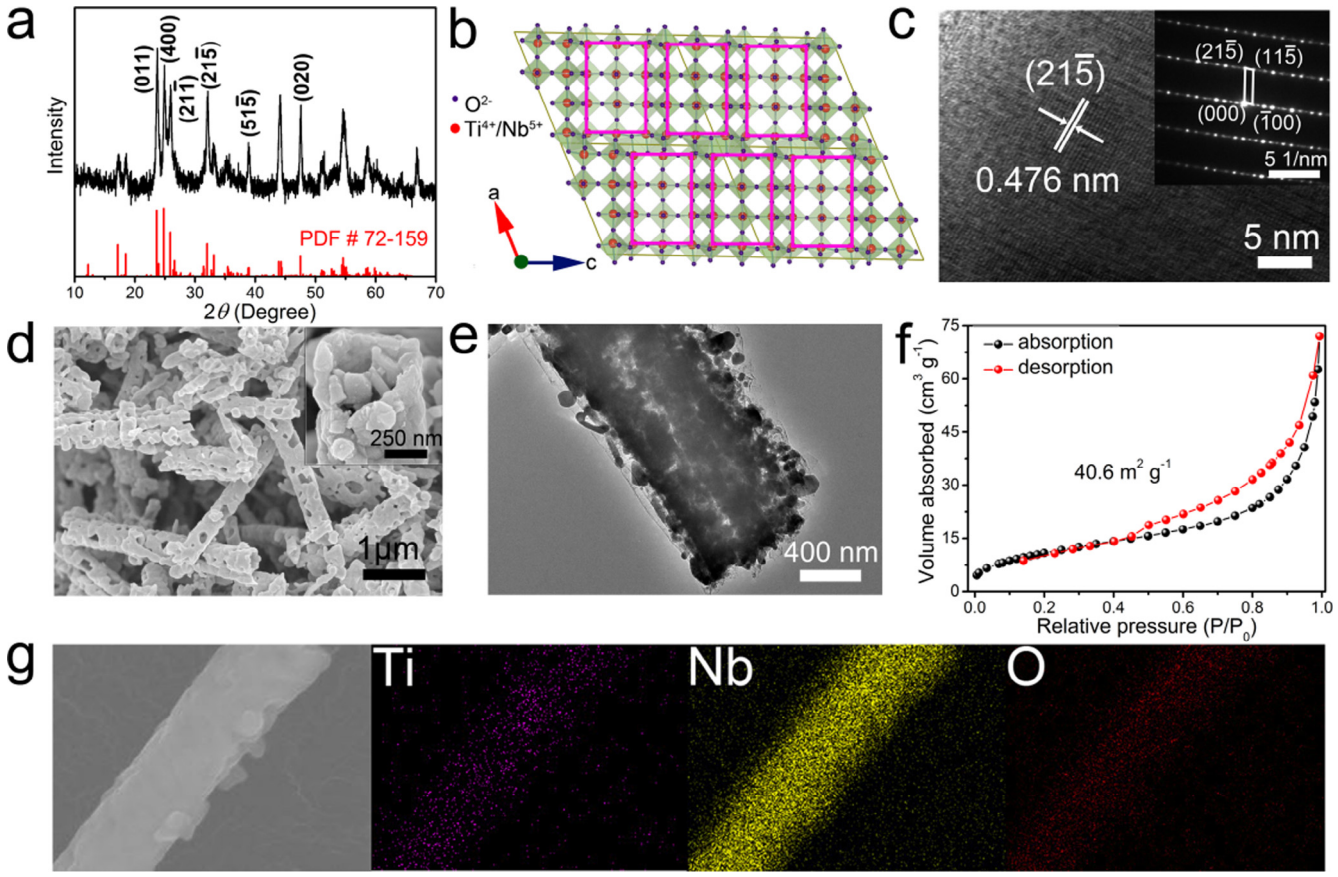

Fig. 1. Material characterizations of $Ti_2Nb_{10}O_{29}$ hollow nanofibers: (a) XRD pattern (no all peaks are indexed due to the large number of peaks), (b) crystal structure, (c) HRTEM image with SAED pattern, (d) FESEM image, (e) TEM image, (f) N_2 adsorption–desorption isotherm and (g) EDX mapping image.

of $Ti_2Nb_{10}O_{29}$. This crystal structure is verified by high-resolution transmission electron microscopy (HRTEM) and selected-area electron diffraction (SAED). The HRTEM image (Fig. 1c) shows an interplanar distance of 0.476 nm, which corresponds to the $(21\bar{5})$ crystallographic plane of $Ti_2Nb_{10}O_{29}$. The SAED pattern (the inset of Fig. 1c) matches with the shear ReO_3 crystal structure of $Ti_2Nb_{10}O_{29}$. The XRD peaks in the $Ti_2Nb_{10}O_{29}$ hollow nanofibers are quite broad, demonstrating their small grain sizes undoubtedly due to the low calcination temperature of 800 °C. However, it is noteworthy that pure $Ti_2Nb_{10}O_{29}$ cannot be obtained when the calcination temperature is below 800 °C (Fig. S1).

The morphology and microstructure of the $Ti_2Nb_{10}O_{29}$ hollow nanofibers are characterized by field emission scanning electron microscopy (FESEM) and TEM. The FESEM image (Fig. 1d) shows that the product possesses a highly porous hollow nanofiber architecture with minor self-aggregation and an average fiber diameter of ~500 nm. From the cross-sectional views (the inset of Fig. 1d and e), the hollow nanofibers are fully constructed by primary nanoparticles, and exhibit rough surfaces and an average shell thickness of ~90 nm. The small primary particles are further supported by the large Brunauer–Emmett–Teller (BET) specific surface area of 40.6 $m^2\ g^{-1}$, obtained from the N_2 adsorption–desorption isotherm of the $Ti_2Nb_{10}O_{29}$ hollow nanofibers (Fig. 1f). The energy-dispersive X-ray (EDX) elemental mapping image of a $Ti_2Nb_{10}O_{29}$ hollow nanofiber (Fig. 1g) reveals the homogeneous Ti, Nb and O distributions in the tested area, confirming the pure $Ti_2Nb_{10}O_{29}$ phase in the hollow nanofibers.

In order to investigate the redox kinetic properties of the $Ti_2Nb_{10}O_{29}$ hollow nanofibers, cyclic voltammetry (CV) measurements are implemented on a half-cell configuration at a low scan speed of 0.2 mV s^{-1} for four cycles within a potential window of 3.0–0.8 V, as presented in Fig. 2a. The position of the sharp cathodic peak shifts from 1.54 V to 1.62 V after the first cycle, which could be explained by the electronic-structure variation of the $Ti_2Nb_{10}O_{29}$ hollow nanofibers rooted in the irreversible lithiation during the first cycle. From the second cycle, the cathodic/anodic shoulder peak-pair at 1.89/1.91 V can be attributed to the valence variations of the Ti^{3+}/Ti^{4+} redox couple; the sharp peak-pair at 1.62/1.70 V can be assigned to the Nb^{4+}/Nb^{5+} redox couple; and the broad bump below 1.4 V can be considered as the subsequent reaction from the Nb^{3+}/Nb^{4+} redox couple. The midpoint between the two sharp peaks at 1.62/1.70 V can correspond to the average working potential of the $Ti_2Nb_{10}O_{29}$ hollow nanofibers. Thus, the working potential is determined to be ~1.66 V, which is slightly lower than the previously reported value (~1.71 V) [9]. This reasonably high working potential inhibits the electrolyte decomposition and lithium-dendrite formation, thereby ensuring a high safety level. It is known that niobium oxides have intrinsic pseudocapacitive behavior, which benefits their capacities and rate capabilities [10]. To quantitatively analyze the pseudocapacitive behavior of the $Ti_2Nb_{10}O_{29}$ hollow nanofibers, the CV experiments are further implemented at 0.4, 0.7 and 1.1 mV s^{-1} (Fig. 2b). The slopes of the $\log(I)$–$\log(v)$ plots for the sharp anodic and cathodic peaks are as large as 0.78 and 0.72, respectively (Fig. 2c), indicating that the electrochemical system is dominated by both the Li^+-ion diffusion and the pseudocapacitive effect. Based on a previously developed calculation method [10], the pseudocapacitive contributions are determined to be 48.2, 54.5, 82.5 and 89.1% at 0.2, 0.4, 0.7